Coherent Detection of Optical Quadrature Phase-Shift Keying Signals With Carrier Phase Estimation

Dany-Sebastien Ly-Gagnon, Satoshi Tsukamoto, Kazuhiro Katoh, and Kazuro Kikuchi, *Member, IEEE, Member, OSA*

***Abstract*—This paper describes a coherent optical receiver for demodulating optical quadrature phase-shift keying (QPSK) signals. At the receiver, a phase-diversity homodyne detection scheme is employed without locking the phase of the local oscillator (LO). To handle the carrier phase drift, the carrier phase is estimated with digital signal processing (DSP) on the homodyne-detected signal. Such a scheme presents the following major advantages over the conventional optical differential detection. First, its bit error rate (BER) performance is better than that of differential detection. This higher sensitivity can extend the reach of unrepeated transmission systems and reduce crosstalk between multiwavelength channels. Second, the optoelectronic conversion process is linear, so that the whole optical signal information can be postprocessed in the electrical domain. Third, this scheme is applicable to multilevel modulation formats such as M-array PSK and quadrature amplitude modulation (QAM). The performance of the receiver is evaluated through various simulations and experiments. As a result, an unrepeated transmission over 210 km with a 20-Gb/s optical QPSK signal is achieved. Moreover, in wavelength-division multiplexing (WDM) environment, coherent detection allows the filtering of a desired wavelength channel to reside entirely in the electrical domain, taking advantage of the sharp cutoff characteristics of electrical filters. The experiments show the feasibility to transmit polarization-multiplexed 40-Gb/s QPSK signals over 200 km with channel spacing of 16 GHz, leading to a spectral efficiency as high as 2.5 b/s/Hz.**

***Index Terms*—Optical fiber communication, phase modulation.**

I. Introduction

MODULATION formats with high spectral efficiency are attractive alternatives for upgrading the capacity of currently deployed transmission links. While the spectral efficiency of binary modulation formats is limited to 1 b/s/Hz/polarization, formats with 2 bits of information per symbol can achieve up to 2 b/s/Hz/polarization of spectral efficiency using half the symbol rate while maintaining the bit rate. For optical communication systems, a reduced symbol rate provides several advantages in terms of tolerance to chromatic dispersion and polarization-mode dispersion (PMD).

Among various modulation formats that carry 2 bits of information per symbol, quadrature phase-shift keying (QPSK) is the most promising because of its superior transmission characteristics [1], [2]. With polarization multiplexing, a bit rate of 40 Gb/s is possible at the symbol rate of 10 Gsymbol/s, so that such a scheme should result in high spectral efficiencies. In recent years, several experiments have investigated the performance of QPSK systems with optical differential detection, where the receiver consisted of two sets of Mach–Zehnder interferometers and balanced photodetectors [3]. However, differential detection of QPSK signals requires an SNR per bit of about 2 dB higher than synchronous coherent detection. If synchronous optical coherent detection is employed, the bit error rate (BER) performance of a QPSK system can ideally match that of a BPSK system, halving the spectral width [4]. In addition, optical coherent detection can rely on the sharp cutoff characteristics of electrical filters to demultiplex adjacent channels in a wavelength-division multiplexed (WDM) system.

To demodulate the QPSK signal, the synchronous coherent receiver must either use a local oscillator (LO) locked to the carrier phase or recover the carrier phase after homodyne detection. Although coherent optical receivers based on an optical phase-locked loop (PLL) have been studied since 1980 [5], the optical PLL is still difficult to achieve, because the practical voltage-controlled oscillator (VCO) operating at the optical stage is not available. On the other hand, electrical digital signal processing (DSP) circuits are becoming increasingly faster and provide simple yet efficient means for estimating the carrier phase [6], [7].

This paper presents the results of our recent developments on an optical receiver that uses coherent detection with phase estimation to demodulate QPSK signals. The in-phase and quadrature components of an optical signal are retrieved using a homodyne phase-diversity receiver without locking the phase of the LO. Our DSP-based phase estimation scheme consists of a simple and demultiplexable architecture that allows the system to reach a significantly higher performance than differential detection. We demonstrate a 210-km unrepeated transmission of a 20-Gb/s QPSK signal, taking advantage of the higher sensitivity of our receiver. Our experiments also show that polarization-multiplexed 40-Gb/s WDM QPSK signals can be transmitted over 200 km with channel spacing of 16 GHz, thus, achieving a spectral efficiency of 2.5 b/s/Hz.

This paper is organized as follows: Section II presents the overall structure of our coherent optical receiver; Section III

Manuscript received June 26, 2005; revised August 23, 2005.

The authors are with the Research Center for Advanced Science and Technology (RCAST), University of Tokyo, Tokyo 153-8904, Japan (e-mail: kikuchi@ginjo.rcast.u-tokyo.ac.jp).

Digital Object Identifier 10.1109/JLT.2005.860477

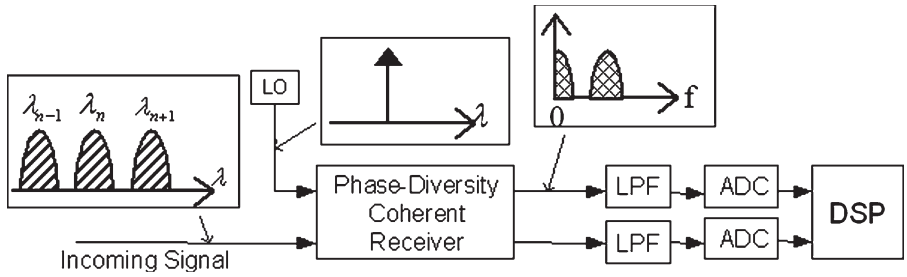

Fig. 1. Structure of the proposed coherent optical receiver.

describes the homodyne phase-diversity receiver that was used in our experiments; Section IV describes the phase estimation scheme with DSP; Sections V and VI present results of our simulations and experiments, respectively; and Section VII is the conclusion of the paper.

II. System Setup Based on Homodyne Detection With Phase Estimation

The setup of our proposed system is shown in Fig. 1. The in-phase and quadrature components of the optical signal are retrieved with a homodyne phase-diversity receiver, and converted to the electrical signals I_{PD1} and I_{PD2}, respectively. Details of the homodyne phase-diversity receiver will be described in Section III. In opposition to direct detection, homodyne detection provides linear optoelectrical conversion. When the LO wavelength is set to λ_n, the channel at a wavelength $\lambda_{(n+1)}$ will overlap the channel at a wavelength $\lambda_{(n-1)}$, but the channel at the selected wavelength λ_n will not be overlapped by any other wavelength channel. Therefore, the two electrical signals I_{PD1} and I_{PD2} can be low-pass filtered to demultiplex the selected wavelength from the incoming signal. The system can benefit from the sharp cutoff characteristics of electrical filters, without the need for any optical filter to filter out the adjacent wavelength channels.

After being filtered, the signals $I_{\mathrm{PD1}}(t)$ and $I_{\mathrm{PD2}}(t)$ are simultaneously sampled once every symbol period T with analog-to-digital converters (ADCs). The sampled signals $I_{\mathrm{PD1}}(n)$ and $I_{\mathrm{PD2}}(n)$, where n denotes the number of the sample, are then processed with DSP circuits. The sampling can be synchronous or asynchronous. When the signal envelope is modulated in the return-to-zero (RZ) waveform, the intensity of RZ pulses can be used as the sampling clock for synchronous sampling. For asynchronous sampling, the signal must be sampled at twice the symbol rate and then resampled to keep one sample per symbol. In both cases, the carrier phase can be evaluated with DSP and used to demodulate the data.

III. Optical Phase-Diversity Homodyne Receiver

The optical phase-diversity homodyne receiver that was used in our experiments is shown in Fig. 2. The receiver uses free-space optical components packaged in a small metal case. Orthogonal states of polarization for the LO and the incoming signal create the 90° hybrid necessary for phase diversity. With the $\lambda/4$ waveplate (QWP), the polarization of the LO becomes

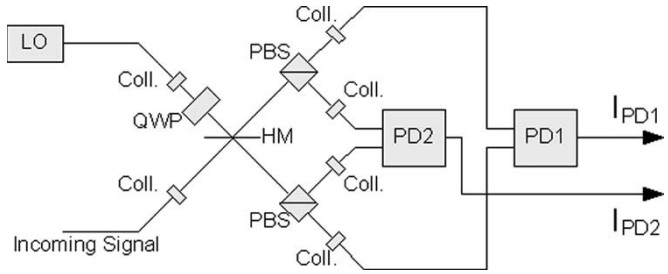

Fig. 2. Construction of the homodyne phase-diversity receiver.

circular, while the signal remains linearly polarized and its polarization angle is 45° with respect to the principal axis of polarization beam splitters (PBSs). After passing through the half mirror (HM), the PBSs separate the two polarization components of the LO and signal while two balanced photodiodes PD1 and PD2 detect the beat between the LO and signal in each polarization.

The complex field of the signal can be represented by

$$E(t) = \sqrt{P_s}\exp\left[j\left(\theta_s(t) + \theta_n(t)\right)\right]$$

where P_s is the signal power, $\theta_s(t)$ the phase modulation $(= 0, \pi/2, \pi, -\pi/2)$, and $\theta_n(t)$ the carrier phase in reference to the LO phase. The currents from PD1 and PD2 are expressed as

$$I_{\mathrm{PD1}}(t) = R\sqrt{P_s P_{\mathrm{LO}}}\cos\left(\theta_s(t) + \theta_n(t)\right)$$
$$I_{\mathrm{PD2}}(t) = R\sqrt{P_s P_{\mathrm{LO}}}\sin\left(\theta_s(t) + \theta_n(t)\right)$$

where R is the responsitivity of the photodiodes and P_{LO} the LO power. The electrical signals I_{PD1} and I_{PD2} contain information on the amplitude and phase of the optical signal.

In this receiver, we have to align the polarization state of the incoming signal, and such polarization alignment is performed manually in our experiments; however, in order to achieve the polarization-independent operation of the receiver, it is possible to introduce polarization diversity by splitting the incoming signal into two orthogonal polarization components and combining them after the electrical conversion. This property stems from the linearity of the system.

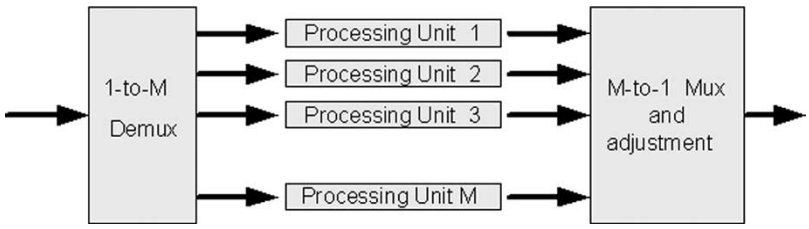

Fig. 3. DSP architecture for phase estimation and demodulation.

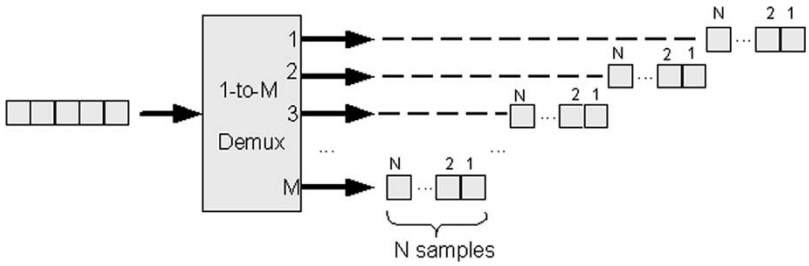

Fig. 4. Schematic of the demultiplexing unit.

IV. Phase Estimation With DSP

Since the linewidth of semiconductor distributed-feedback (DFB) lasers used as the transmitter and LO typically ranges from 100 kHz to 10 MHz, the optical carrier phase $\theta_n(t)$ varies much more slowly than the phase modulation, whose symbol rate is 10 Gsymbol/s in our experiments. Therefore, by averaging the carrier phase over many symbol intervals, it is possible to obtain an accurate phase estimate, as shown in the following. In such a case, coherent detection will offer significant improvement of BER performance over differential detection.

The reconstructed signal samples $E(n) = [I_{\mathrm{PD1}}(n) + jI_{\mathrm{PD2}}(n)]$, where n denotes the number of samples, are processed in a DSP circuit. A block diagram of the DSP circuit is shown in Fig. 3. The circuit consists of a demultiplexing unit, several processing units (PUs) that estimate the phase and demodulate the data, and a remultiplexing unit. The stream of $E(n)$ are demultiplexed into M blocks of N samples (as shown in Fig. 4) before being sent to the PUs. The core processing functions residing in the PUs can demodulate the data in parallel and independently from each other, which allows this architecture to support high symbol rates.

A schematic of a PU is shown in Fig. 5. $E(i)$ $(i = 1, \ldots, N)$ to the fourth power cancels the phase modulation θ_s $(= 0, \pi/2, \pi, -\pi/2)$, since $E^4 \propto \exp[j(4\theta_n)]$. The complex amplitudes E^4 are summed, so that the phase is averaged over the entire block. The phase of the resulting complex amplitude is divided by 4, leading to a phase estimate θ_e that lies between $-\pi/4$ and $\pi/4$. The phase estimate θ_e is, thus, given as

$$\theta_e = \frac{1}{4} \arg \left[\sum_{i=1}^{N} E^4(i) \right].$$

Discriminating the phase $\theta_s = [\arg(E(i)) - \theta_e]$ of the ith sample among four states results in a symbol $t_i (= 00, 01, 11, \text{ or } 10)$.

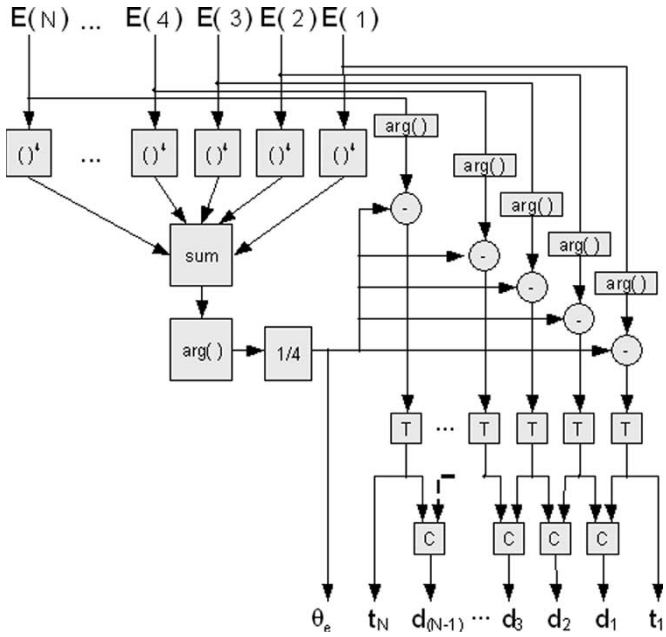

Fig. 5. Schematic of the PU that estimates the phase and demodulates the data. T represents the threshold detector and C the comparator.

It is important to note that the data are differentially precoded, even if we do not employ differential detection. For synchronous coherent detection, differential precoding can solve the phase ambiguity, as an alternative to periodically sending a synchronization sequence. Comparing the symbol t_i $(i < N)$ with the symbol $t_{(i+1)}$, we obtain the differentially decoded symbol d_i. The $(N-1)$ data symbols d_i are passed to the remultiplexing unit, along with the phase estimate θ_e and the symbols t_1 and t_N.

The remultiplexing unit is shown in Fig. 6. The phase estimate from the mth PU is denoted as $\theta_e(m)$. The data symbol d_N at the boundary between the $(m-1)$th PU and the mth PU will be adjusted by using the phase estimates $\theta_e(m)$

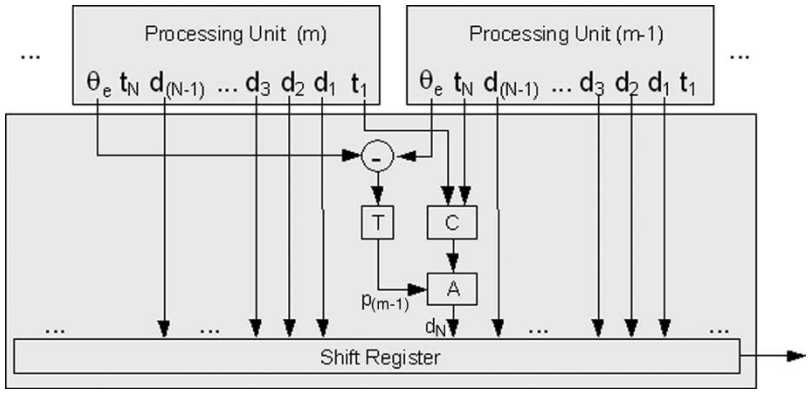

Fig. 6. Schematic of the remultiplexing unit. T, C, and A represent the threshold detector, comparator, and adder, respectively. $p(m-1)$ adjusts the last symbol d_n from the $(m-1)$th PU, depending on whether $[\theta_e(m) - \theta_e(m-1)]$ is greater than $+\pi/4$ or less than $-\pi/4$.

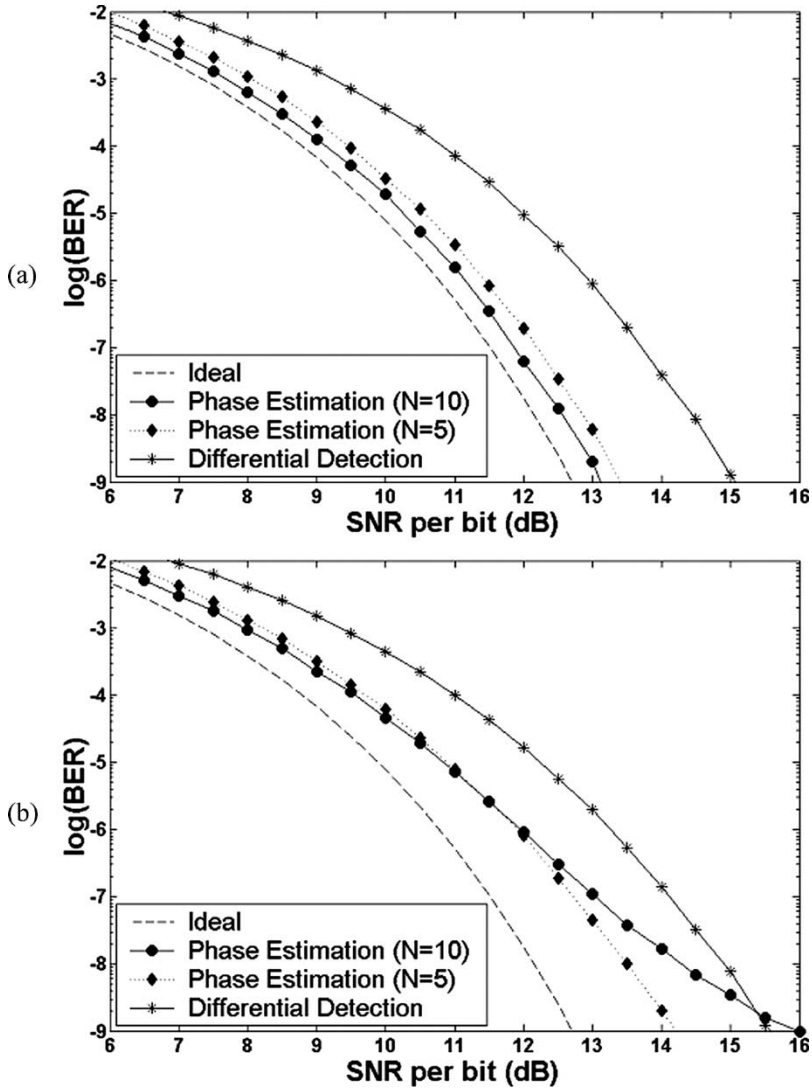

Fig. 7. Simulation results of the BER performance. Laser linewidths of (a) 325 kHz ($\sigma_s = 0.02$ at 10 Gsymbol/s) and (b) 2 MHz ($\sigma_s = 0.05$ at 10 Gsymbol/s).

and $\theta_e(m-1)$ as follows: If the phase difference $[\theta_e(m) - \theta_e(m-1)]$ is less than $-\pi/4$ (or greater than $+\pi/4$), the first decoded symbol becomes the next (or previous) symbol of the QPSK constellation. $p(m-1)$ in Fig. 6 shows such shift of the symbol. This adjustment ensures that the phase estimates follow the trajectory of the physical phase [6]. The shift register serializes the decoded data symbols from d_1 to d_N of the $(m-1)$th PU, followed by the data symbols from d_1 to d_N of the mth PU, and loops across the mth PU to remultiplex the decoded data symbols.

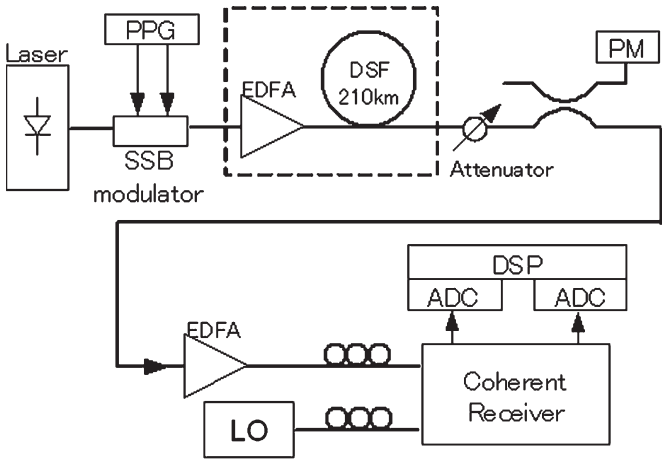

Fig. 8. Experimental setup for investigating the BER performance.

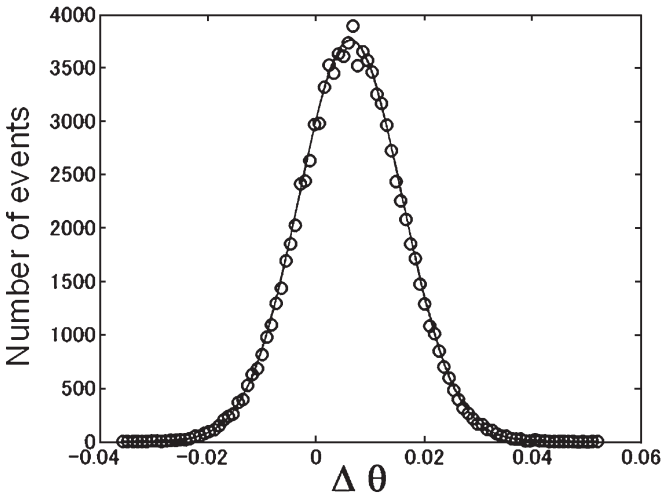

Fig. 9. Histogram of the phase difference $\Delta\theta$ in a time interval of 50 ps. Dots are measured values and the solid curve is a Gaussian fit.

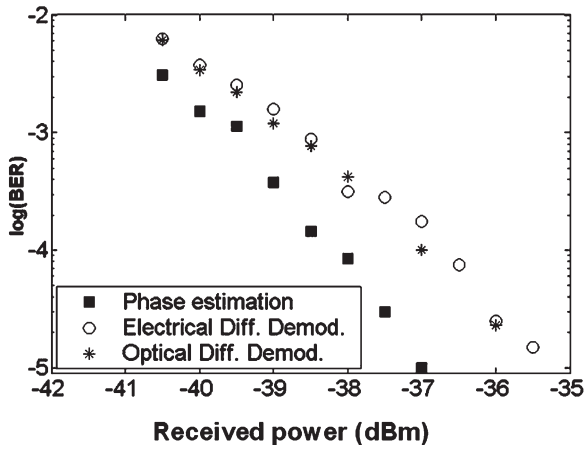

Fig. 10. Back-to-back BER performance measured with phase estimation and differential demodulation (both electrical and optical).

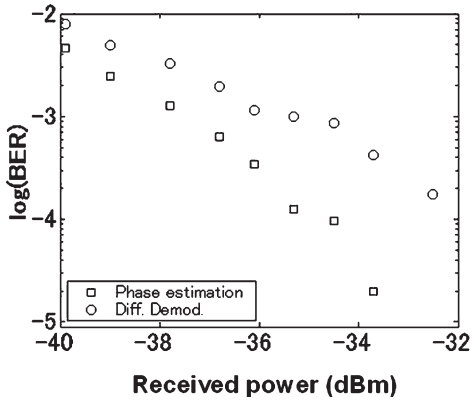

Fig. 11. BER performance after 210 km of transmission measured with phase estimation and differential demodulation.

V. Simulations

In this section, we calculate BER performance of the phase estimation scheme and the differential detection scheme for different levels of SNR per bit, using Monte Carlo simulations. We assume that the phase difference $\theta_n(t+T)-\theta_n(t)$ in a symbol interval T follows a Gaussian distribution with a variance $\sigma_p^2 = 4\pi\Delta f T$, where Δf denotes the spectral width of the transmitter and LO [8].

Fig. 7 shows BER curves for phase estimation and differential detection at appropriate block lengths. We assume that $\sigma_p = 0.02$ in Fig. 7(a) and $\sigma_p = 0.05$ in Fig. 7(b), which correspond to a sum of laser linewidths of $2\Delta f = 325$ kHz and $2\Delta f = 2.0$ MHz, respectively, at 10 Gsymbol/s. Fig. 7(a) shows that the phase estimation scheme outperforms the differential detection scheme, and the BER curve of the phase estimation scheme is close to the ideal case without phase noise, when a block length $N = 10$. We find that the larger block length gives us the better BER performance, because the estimated phase has less fluctuation owing to a larger number of averaged samples. However, when the phase drift becomes larger, a good BER performance cannot be achieved if N is too large. This is due to the fact that the phase difference between the first and last samples of the block becomes significant. Fig. 7(b) presents such case, where a block length of $N = 10$ is too large, but $N = 5$ is appropriate if a BER of 10^{-9} is required. Therefore, it is important to find the optimal block length depending on the property of the laser phase noise.

In the abovementioned simulation, we did not take the beat-frequency offset δf into account; however, we find that the offset-induced phase deviation in a block $2\pi\delta f T N$ should be smaller than 5°, which means that the allowable frequency offset is about 10 MHz for $N = 10$.

VI. Experiments

A. Laser Phase Noise Measurement

Using the setup shown in Fig. 8, we characterized the phase noise of our DFB lasers, collecting samples at the ADCs when the optical signal was not modulated and the fiber link was not inserted. The laser bias and temperature of the transmitter and LO were maintained through a feedback loop so that the frequency drift becomes lower than 10 MHz. At the receiver, the optical signal went through the coherent receiver and was detected with two balanced photodiodes PD1 and PD2, as described in Section III. The signals I_{PD1} and I_{PD2} were

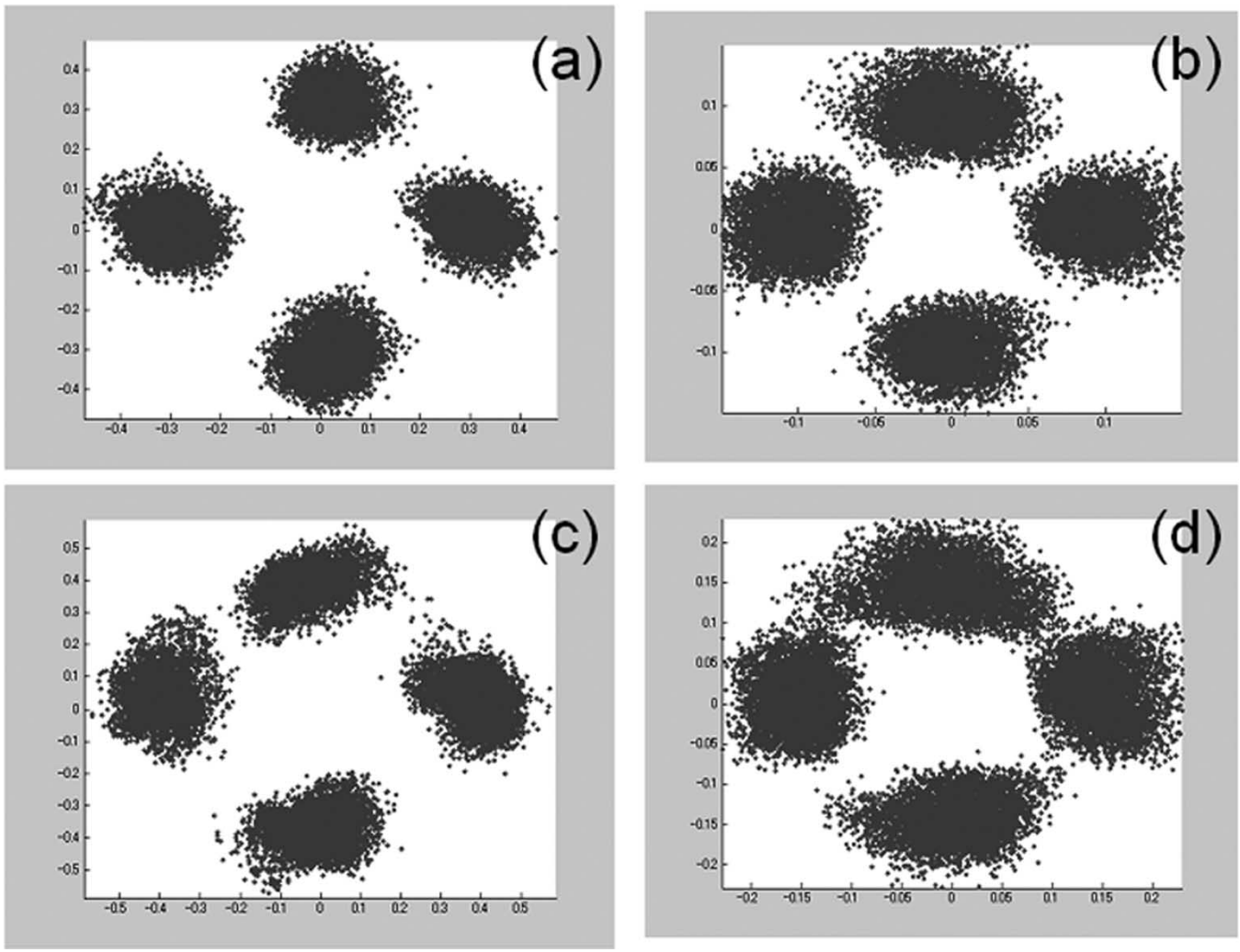

Fig. 12. Complex amplitude after 210 km of transmission. (a), (b) Measured with phase estimation and differential demodulation, respectively, when $P_{\rm in} = 12$ dBm. (c), (d) Measured when $P_{\rm in} = 13.5$ dBm.

simultaneously sampled at a rate of 20 Gsample/s with ADCs embedded within a Tektronix TDS6804B oscilloscope.

The carrier phase $\theta_n(t)$ exhibited random fluctuation in time. The histogram of the phase difference $\Delta\theta = \theta_n(t+T) - \theta_n(t)$ measured in a period T of 50 ps (circles) is shown in Fig. 9 along with a Gaussian distribution fit (solid curve). The distribution agrees well with the Gaussian fit having the variance $\sigma_p^2 = 9.1 \times 10^{-5}$, which corresponds a linewidth Δf of about 150 kHz.

B. Back-to-Back BER Measurement

The back-to-back BER was measured by using the experimental setup shown in Fig. 8, where the fiber link was not inserted. Two data tributaries were precoded at the pulse pattern generator (PPG) such that differential decoding of the transmitted data resulted in two PRBS7 sequences delayed by 63 symbols. The DFB laser output was modulated through a $LiNbO_3$ single-sideband (SSB) modulator at a bit rate of 2×10 Gb/s. The received power was adjusted with an attenuator and monitored with a power meter (PM). The received signal was amplified with an erbium-doped fiber amplifier (EDFA) to -10 dBm before it was detected with the coherent receiver. The polarization state of the incoming signal was adjusted manually.

The BER measurement was performed off-line. The collected samples were resampled to keep only one point per symbol and combined to form an 80-ksymbol-long stream. The number of errors was counted from these streams to determine the BER. However, the real-time signal processing will be possible by using a dedicated integrated circuit.

The receiver sensitivity of the system using phase estimation is compared with that using differential detection in Fig. 10. For phase estimation, the accumulated samples were demodulated as explained in Section IV with a block length of $N = 10$. For electrical differential detection, the phase difference between two samples was used to decode the information. As a reference, the BER performance of optical differential detection with a Mach–Zehnder interferometer is also shown by stars in Fig. 10. Its performance is very similar to the differential detection with the coherent receiver. The receiver sensitivity of the phase estimate method is about 1.5 dB better than that of the differential detection method at BER of 10^{-5}, as predicted by Fig. 7(a).

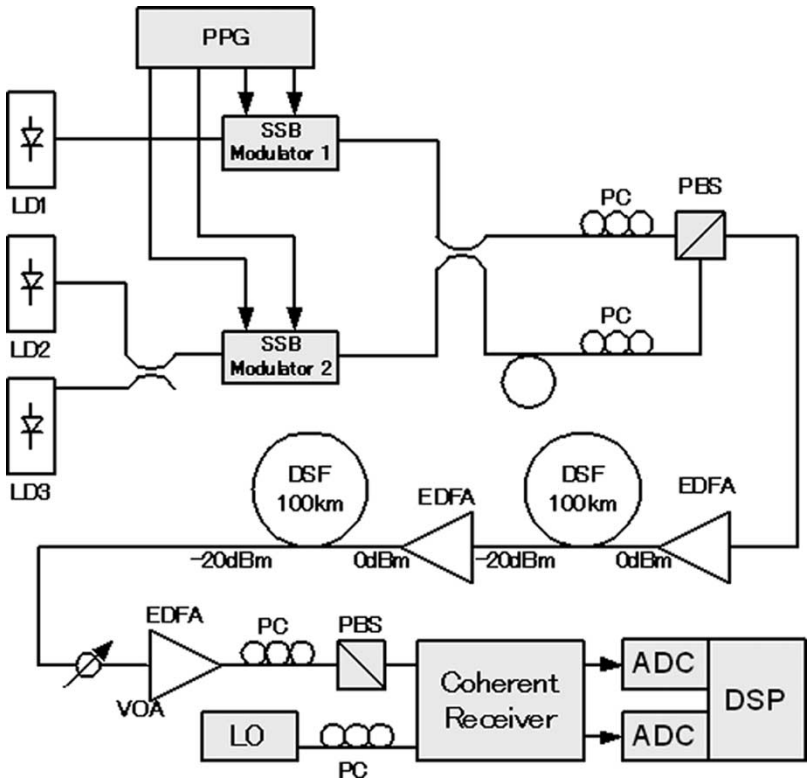

Fig. 13. Experimental setup for polarization-multiplexed 40-Gb/s WDM QPSK transmission.

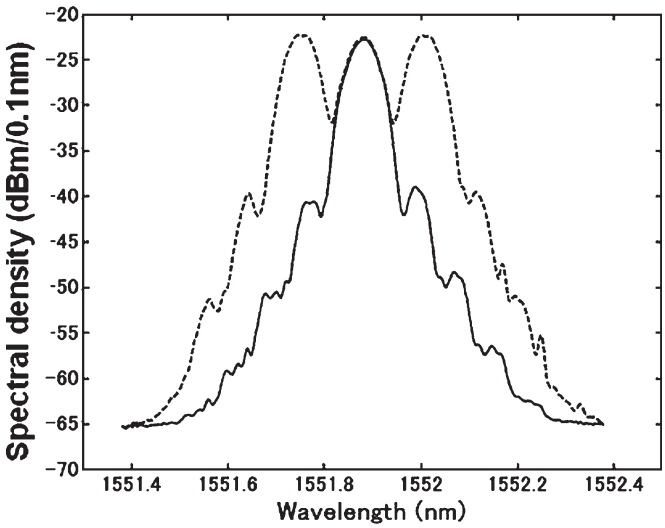

Fig. 14. Optical spectrum of three WDM channels with 16-GHz spacing.

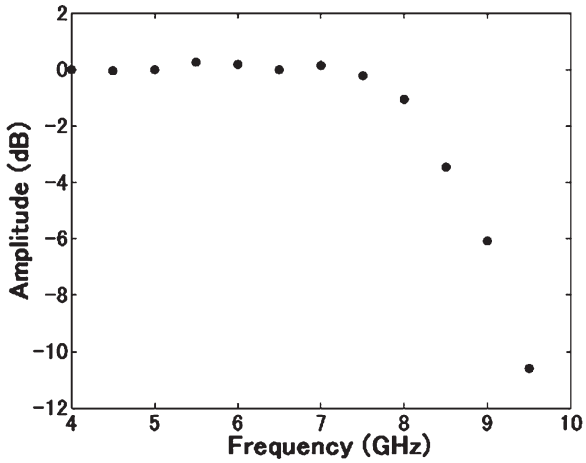

Fig. 15. Filtering characteristics of the low-pass electrical filters.

C. 210-km Unrepeated Transmission Experiment

We used the experimental setup depicted by Fig. 8 to transmit a QPSK signal over an unrepeated fiber span of 210 km. The 20-Gb/s QPSK signal was amplified to the power of $P_{\rm in}$ by an EDFA before propagating through the unrepeated span of 210 km of dispersion-shifted fiber (DSF). Fig. 11 shows the BER curves after 210 km of transmission. $P_{\rm in}$ is fixed to 12 dBm, at which the transmission impairment due to fiber nonlinearity is not serious.

Our coherent receiver also offers a straightforward method of monitoring the transmitted signal quality by plotting the complex amplitude of the signal on the two-dimensional (2-D) complex plane. Fig. 12(a) and (b) shows distributions of the complex amplitude after 210-km propagation, which are obtained with phase estimation and differential demodulation, respectively. The received power in this case is -32.5 dBm. When the phase estimation is employed, the distribution of the complex amplitude is clearly separated into four regions as shown in Fig. 12(a), and no error is recorded throughout the streams of 80 kb, leading to a BER smaller than 1.25×10^{-5}.

On the other hand, differentially demodulating the same samples presents a BER around 2×10^{-4} due to the larger phase noise involved in the demodulation process [Fig. 12(b)]. The BER performance of the 20-Gb/s QPSK signal after unrepeated

210 km of transmission is, therefore, drastically improved with phase estimation as shown in Fig. 11. When $P_{\rm in}$ is increased above 13.5 dBm, fiber nonlinearity begins to cause severe transmission impairment. The phase noise enhancement can be observed with the phase estimation as shown in Fig. 12(c) but is not clear in Fig. 12(d) with differential demodulation.

D. 40-Gb/s WDM Experiment

To investigate the performance of coherent detection with phase estimation in a WDM environment, the setup shown in Fig. 13 was implemented. Three DFB semiconductor lasers (LD1, LD2, and LD3) oscillating at wavelengths around 1.55 μm were used as transmitters. Their channel spacing was set to exactly 16 GHz by monitoring the beat of the coherently detected spectrum. The center channel and the adjacent channels were modulated with two $LiNbO_3$ SSB modulators (SSB modulator 1 and SSB modulator 2). Each modulator was independently driven with two precoded streams of 10-Gb/s electrical signals, resulting in optical 20-Gb/s QPSK signals. The three channels were combined with polarization-maintaining (PM) couplers. One of the outputs of the second PM coupler was polarized orthogonally with respect to the other through polarization controllers (PCs) and then recombined with a PBS. One arm had a relative delay of several nanoseconds for decorrelation. This transmitter setup resulted in a polarization-multiplexed 40-Gb/s QPSK signals. The signal power was boosted to 0 dBm per channel by an EDFA. The spectrum of the launched signal is shown in Fig. 14. All the channels were kept at an equal power and launched on two 100-km spans of DSF connected by an EDFA. The loss of each 100-km span was about 20 dB.

The received signal power was controlled by a variable optical attenuator (VOA) and amplified by a single EDFA before detection. At the first stage of the receiver, polarization demultiplexing was realized with a PC and a PBS. While polarization tracking would be necessary in a real system, it was not employed in this experiment. The frequency of the LO was tuned to that of LD1 to select the center channel.

The ADCs themselves had low-pass filter (LPF) characteristics with a cutoff frequency of around 8 GHz, as shown in Fig. 15. The two electrical signals $I_{\rm PD1}$ and $I_{\rm PD2}$ were, therefore, band limited, which resulted in the elimination of the amplifier noise and a reduction of the crosstalk from the adjacent channels. Note that we did not use any optical bandpass filter for demultiplexing the WDM channels.

We first measured the back-to-back BER of a single wavelength with and without polarization multiplexing to assess the penalty due to the introduction of polarization multiplexing. In Fig. 16, dots and circles show the BER as a function of the received power P_r when the center channel is restored with (a) phase estimation and (b) differential demodulation. From these figures, we can see that the power penalty due to polarization multiplexing is very small, because the orthogonality of the two polarization states can be well maintained and the PBS has a polarization extinction ratio of about 25 dB. In addition, note that phase estimation outperforms differential demodulation by about 4 dB at BER $= 10^{-5}$.

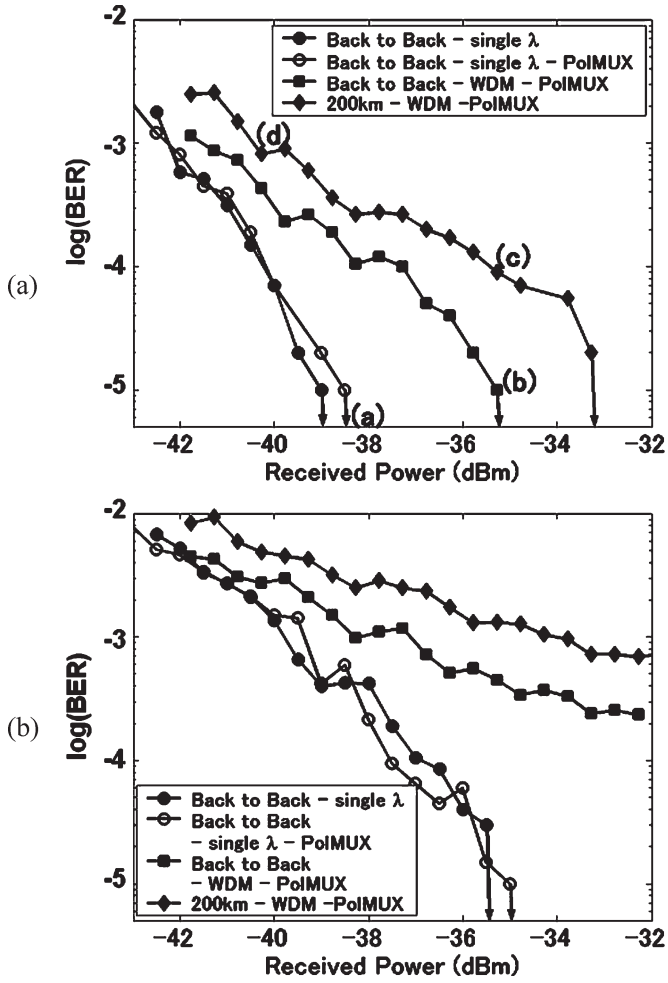

Fig. 16. BER as a function of the received power with (a) phase estimation and (b) differential detection.

Next, we evaluated WDM performance with polarization multiplexing. Squares and diamonds in Fig. 16 show the back-to-back BERs and the BER after 200 km of transmission. The phase estimation scheme greatly mitigates the effect of interchannel crosstalk. In fact, in the WDM system, we can achieve error-free operation only with phase estimation, although the crosstalk penalty is about 3 dB at BER $= 10^{-5}$ as shown in Fig. 16(a). On the other hand, the penalty after 200 km of transmission of the polarization-multiplexed WDM channel is about 2 dB. PMD might be one of the reasons for such a transmission penalty. Thus, we achieve a spectral efficiency of 2.5 b/s/Hz.

Fig. 17 shows distributions of the complex amplitude of the transmitted QPSK signals for the four cases (a)–(d) indicated in Fig. 16, showing the quality of QPSK signals visually.

VII. Conclusion

We have investigated coherent optical detection with phase estimation for demodulating a 10-Gsymbol/s optical QPSK signal. The carrier phase is estimated with DSP, alleviating locking the phase of the LO to the carrier phase. Through simulations and experiments, we have found that the phase

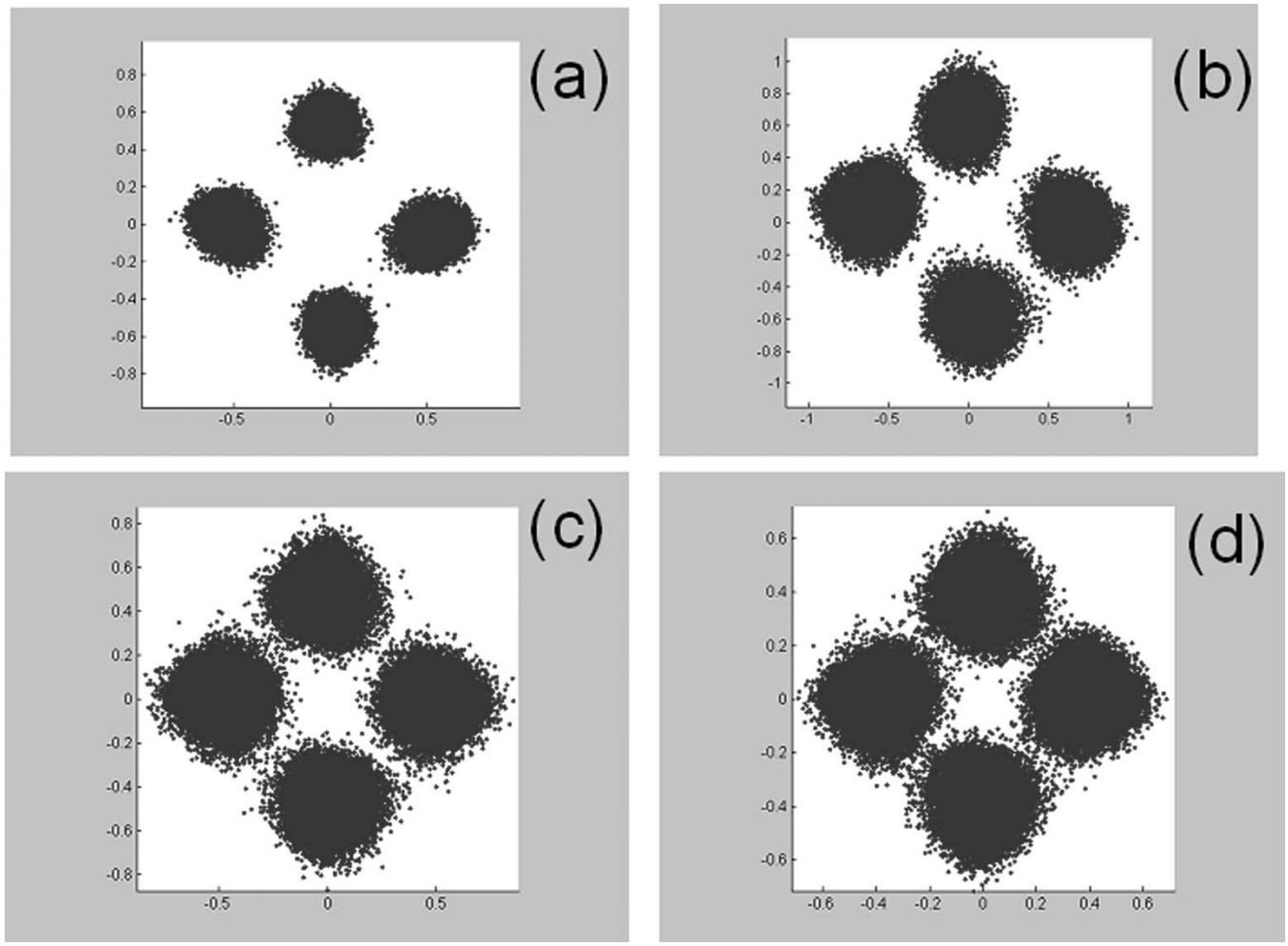

Fig. 17. Distribution of the complex amplitude on the complex plane. (a) $P_r = -35.0$ dBm (single λ). (b) $P_r = -35.2$ dBm (WDM). (c) $P_r = -35.2$ dBm (WDM after 200 km). (d) $P_r = -40.2$ dBm (WDM after 200 km).

noise of present-state-of-the-art semiconductor DFB lasers is substantially small such that an accurate phase estimate can be obtained from the sampled signal at the symbol rate of 10 Gsymbol/s.

We have also found that the receiver sensitivity of such a system is significantly improved in comparison to differential detection. The higher sensitivity extends the reach of a 20-Gb/s QPSK unrepeated transmission system. In a WDM system, the entire wavelength demultiplexing could be achieved electrically. The spectral efficiency of 2.5 b/s/Hz was demonstrated by a WDM transmission of polarization-multiplexed 40-Gb/s QPSK signals with 16-GHz spacing, although the BER was estimated from the off-line measurement.

The combination of multibit per symbol modulation formats, WDM with narrow channel spacing, and polarization multiplexing is attractive for increasing the spectral efficiency in a cost-effective manner. For this purpose, our coherent receiver will play an important role.

REFERENCES

[1] J. Kahn and K.-P. Ho, "Spectral efficiency limits and modulation/detection techniques for DWDM systems," *IEEE J. Sel. Topics Quantum Electron.*, vol. 10, no. 2, pp. 259–272, Mar./Apr. 2004.

[2] C. Xu, X. Liu, and X. Wei, "Differential phase-shift keying for high spectral efficiency optical transmissions," *IEEE J. Sel. Topics Quantum Electron.*, vol. 10, no. 2, pp. 281–293, Mar./Apr. 2004.

[3] R. Griffin and A. Carter, "Optical differential quadrature phase-shift key (oDQPSK) for high capacity optical transmission," in *Proc. Optical Fiber Communication Conf. (OFC)*, Anaheim, CA, Mar. 2002, pp. 17–22, Paper WX6.

[4] J. Proakis, *Digital Communications*, 4th ed. New York: McGraw-Hill, 2000.

[5] T. Okoshi and K. Kikuchi, *Coherent Optical Fiber Communications*. Boston, MA: Kluwer, 1988.

[6] R. Noe, "Phase noise tolerant synchronous QPSK receiver concept with digital I&Q baseband processing," in *Proc. Opto-Electronics and Communications Conf. (OECC)*, Yokohama, Japan, Jul. 12–16, 2004, pp. 818–819.

[7] D. S. Ly-Gagnon, K. Katoh, and K. Kikuchi, "Unrepeatered optical transmission of 20 Gb/s quadrature phase-shift keying signals over 210 km using homodyne phase-diversity receiver and digital signal processing," *Electron. Lett.*, vol. 41, no. 4, pp. 59–60, Feb. 2005.

[8] K. Kikuchi, T. Okoshi, M. Nagamatsu, and N. Henmi, "Degradation of bit-error rate in coherent optical communications due to spectral spread of the transmitter and the local oscillator," *J. Lightw. Technol.*, vol. LT-2, no. 6, pp. 1024–1033, 1984.

Dany-Sebastien Ly-Gagnon, photograph and biography not available at the time of publication.

Satoshi Tsukamoto, photograph and biography not available at the time of publication.

Kazuhiro Katoh, photograph and biography not available at the time of publication.

Kazuro Kikuchi (M'90) was born in Miyagi Prefecture, Japan, on March 6, 1952. He received the B.S. degree in electrical engineering and the M.S. and Ph.D. degrees in electronic engineering from the University of Tokyo, Tokyo, Japan, in 1974, 1976, and 1979, respectively.

In 1979, he joined the Department of Electronic Engineering at the University of Tokyo. In 1997, he moved to the Research Center for Advanced Science and Technology (RCAST) at the same university. From April 1986 to March 1987, he was on leave of absence from the University of Tokyo with Bell Communications Research (Bellcore), Red Bank, NJ. Since 1979, his work has been on the optical communication system. He is currently involved in optical signal processing devices and their applications to systems. He is also interested in coherent optical communication systems that realize multilevel modulation formats with high spectral efficiency.

Dr. Kikuchi is a member of the Optical Society of America (OSA) and the Institute of Electronics, Information and Communication Engineers (IEICE) of Japan.